Mater Renew Sustain Energy (2014) 3:18
DOI 10.1007/s40243-013-0018-x

ORIGINAL PAPER

Preparation and electrochemical characterization of $(100 - x)(0.7Li_2S{\cdot}0.3P_2S_5){\cdot}xLiBr$ glass–ceramic electrolytes

Satoshi Ujiie · Akitoshi Hayashi · Masahiro Tatsumisago

Received: 19 July 2013 / Accepted: 23 October 2013 / Published online: 19 November 2013

Abstract Glass and glass–ceramic electrolytes of $(100 - x)(0.7Li_2S{\cdot}0.3P_2S_5){\cdot}xLiBr$ ($x = 0$, 5, 10, 12.5, 15 and 20) (mol %) were synthesized by mechanical milling and subsequent heat treatment. Glass powders with no crystal phase were obtained by mechanical milling. The conductivities of the glasses increased concomitantly with increasing LiBr content. The conductivity at $x = 20$ was 3.1×10^{-4} S cm^{-1} at room temperature. The $Li_7P_3S_{11}$ crystal with high Li ion conductivity was precipitated in the glass–ceramics obtained by heat treatment. LiBr crystal was also precipitated in the glass–ceramics containing LiBr as a starting material. The glass–ceramic at $x = 10$ showed conductivity of 6.4×10^{-3} S cm^{-1}. It increased to 8.4×10^{-3} S cm^{-1} by control of the milling period to prepare the precursor glass. $90(0.7Li_2S{\cdot}0.3P_2S_5){\cdot}10LiBr$ glass–ceramic with high Li ion conductivity had a wide electrochemical window of 10 V. An all-solid-state lithium secondary battery using $90(0.7Li_2S{\cdot}0.3P_2S_5){\cdot}10LiBr$ glass–ceramic as an electrolyte was charged and discharged successfully.

Keywords Solid electrolyte · Glass–ceramic · Sulfide · Lithium ion conductivity · Lithium battery

S. Ujiie · A. Hayashi (✉) · M. Tatsumisago
Department of Applied Chemistry, Graduate School of Engineering, Osaka Prefecture University, 1 - 1 Gakuencho, Naka-ku, Sakai, Osaka 599-8531, Japan
e-mail: tatsu@chem.osakafu-u.ac.jp

S. Ujiie
Energy Use R&D Center, The Kansai Electric Power Co., Inc, 11-20-3 Nakoji Amagasaki, Hyogo 661-0974, Japan

Introduction

Electric power generation using renewable energy such as sunlight and wind is increasing. Electrical storage will be an important function of the power system because power is not supplied continuously by such renewable energy resources. Batteries are suitable for power storage because of their high energy efficiencies. Lithium ion batteries with high energy densities are expected to be used in large-scale power storage systems. Safety and reliability are strongly required for large storage systems, while lithium ion batteries present the risk of burning because of their flammable liquid electrolytes. All-solid-state batteries using non-flammable solid electrolytes are expected to improve the safety and reliability of lithium ion batteries. However, the conductivities of the solid electrolytes are not sufficiently high. Solid electrolytes with high lithium ion conductivities and wide electrochemical windows are necessary to put all-solid-state batteries to practical use.

Sulfide-based electrolytes as lithium ion conductors have been investigated [1–12]. The crystals in the Li_2S–GeS_2–P_2S_5 system called thio-LISICON have conductivities of 10^{-4}–10^{-3} S cm^{-1} at room temperature [5]. Recently, Kanno et al. [13] reported a new crystal of $Li_{10}GeP_2S_{12}$ showing extremely high conductivity of 1.2×10^{-2} S cm^{-1}. The glass electrolytes in the Li_2S–P_2S_5 system have conductivities of 10^{-4} S cm^{-1} at room temperature. They are enhanced by the addition of a lithium halide [1]. The lithium ion conductivity of $70Li_2S{\cdot}30P_2S_5$ glass increased from 1.3×10^{-4} to 5.6×10^{-4} S cm^{-1} by the addition of 20 mol % LiI [14]. Presumably, the enhancement of conductivity resulted from the increase of the total lithium ion concentration in the glass. The glass–ceramic electrolytes in the Li_2S–P_2S_5 system also show high lithium ion conductivities [6–9].

Above all, $70Li_2S{\cdot}30P_2S_5$ glass–ceramic containing the $Li_7P_3S_{11}$ crystal has high conductivity of 4.2×10^{-3} S cm^{-1} [6]. We added LiI to the $70Li_2S{\cdot}30P_2S_5$ glass–ceramic in expectation of increased conductivity, but the conductivity decreased sharply with increasing LiI contents [14]. Unknown crystal phase was precipitated in the glass–ceramic added with LiI, although the fraction of the $Li_7P_3S_{11}$ crystal with high conductivity decreased. A solid solution of LiI in the $Li_7P_3S_{11}$ crystal was not confirmed. The conductivity of the $70Li_2S{\cdot}30P_2S_5$ glass–ceramic would be enhanced if the lithium ion concentration could be increased without decreasing the $Li_7P_3S_{11}$ crystal phase.

In this study, LiBr was added to the $70Li_2S{\cdot}30P_2S_5$ glass–ceramic. The effective ionic radii of I^-, Br^- and S^{2-} are, respectively, 220, 196 and 184 pm [15]. LiBr might be dissolved in the $Li_7P_3S_{11}$ crystal because the radius of Br^- is smaller than that of I^-; moreover, it is close to that of S^{2-}. The solid solution is expected to reduce the precipitation of other crystal phases that would decrease the glass–ceramic conductivity. The addition of LiBr increases the Li content in the $70Li_2S{\cdot}30P_2S_5$ glass–ceramic. It is therefore expected that the addition of LiBr to the $70Li_2S{\cdot}30P_2S_5$ glass–ceramic enhances the conductivity. We synthesized the glass–ceramic electrolytes by mechanical milling and subsequent heat treatment. The crystalline phases and the conductivities of the glass–ceramics were examined. An all-solid-state cell was fabricated. Then its charge–discharge performance was investigated.

Experimental

$(100 - x)(0.7Li_2S{\cdot}0.3P_2S_5){\cdot}x$LiBr (mol %) ($x = 0$, 5, 10, 12.5, 15 and 20) glasses were synthesized by mechanical milling. Reagent-grade Li_2S (99.9 %; Nippon Chemical Ind. Co. Ltd.), P_2S_5 (99 %; Aldrich Chemical Co. Inc.) and LiBr (99.999 %; Aldrich Chemical Co. Inc.) were used as starting materials. They were mixed in an agate mortar for 10 min and put into a 45 ml ZrO_2 pot with 500 ZrO_2 balls of 4 mm diameter. The pot was mounted on a planetary ball mill apparatus (Pulverisette 7; Fritsch GmbH). Then the materials were milled at 500 rpm for 10 or 20 h. Some samples labeled as "$(A + B) + C$" were synthesized using two-step milling: A and B were mixed and milled for 10 h, then the obtained compound and C were mixed and milled for 10 h. All processes were conducted in a dry Ar atmosphere. Glass–ceramic samples were obtained by heating the milled samples.

Differential thermal analyses (DTA) were conducted using a thermal analyzer (Thermo-plus 8120; Rigaku Corp.) to observe crystallization temperatures. The glass samples were sealed in Al pans in an Ar-filled glove box and heated at 10 °C min^{-1} under N_2 gas flow up to 400 °C. X-ray diffraction (XRD) measurements (CuKα) were performed using a diffractometer (SmartLab; Rigaku Corp.) to identify crystal phases of the glass samples and the glass–ceramic samples. Ionic conductivities were measured for the pelletized samples pressed under 360 MPa. The pellet diameter and thickness were, respectively, 10 mm and about 1.5 mm. Carbon paste was painted as electrodes on both faces of the pellets and stainless steel disks were attached to the pellets as current collectors. The prepared two-electrode cell was packed in a silica glass tube. Then AC impedances were measured under dry Ar gas flow using an impedance analyzer (1260; Solartron Analytical). The frequency range and the applied voltage were, respectively, 10 Hz to 8 MHz and 50 mV. The electrochemical stability of the glass–ceramic sample was evaluated using cyclic voltammetry at room temperature using a potentiostat (1287; Solartron Analytical). A stainless steel disk as a working electrode and a lithium metal foil as a counter and reference electrode were attached to each face of the pelletized sample. The potential was swept between −0.1 and +10 V with a scanning rate of 5 mV s^{-1}. An all-solid-state two-electrode cell was assembled using the glass–ceramic sample as an electrolyte. The positive electrode was prepared by mixing two powders of $LiCoO_2$ as an active material and the glass–ceramic as an electrolyte. The $LiCoO_2$ particles were coated with $LiNbO_3$ thin film in advance because the $LiNbO_3$-coated $LiCoO_2$ shows good charge–discharge performance in all-solid-state batteries using a sulfide-based electrolyte [16]. An indium foil was used as a negative electrode.

Results and discussion

The XRD patterns of the $(100 - x)(0.7Li_2S{\cdot}0.3P_2S_5){\cdot}x$LiBr samples prepared by mechanical milling for 10 h are presented in Fig. 1. Halo patterns were observed for all the samples, indicating that amorphous powders with no crystal phase were obtained in the composition of $0 \leq x \leq 20$.

Figure 2 shows the DTA curves of the milled samples. Glass transition phenomena occurred between 180 and 220 °C, which suggested that the amorphous powders obtained by milling were glasses. Marked exothermic peaks were observed between 230 and 260 °C. These peaks were regarded as resulting from crystallization of the glasses because the samples heated to temperatures just above these temperatures exhibited crystalline XRD patterns as depicted in Fig. 3. The glass transition temperatures and the crystallization temperatures were shifted to a lower temperature with increasing LiBr content. The shifts of the temperatures would result from the change of the

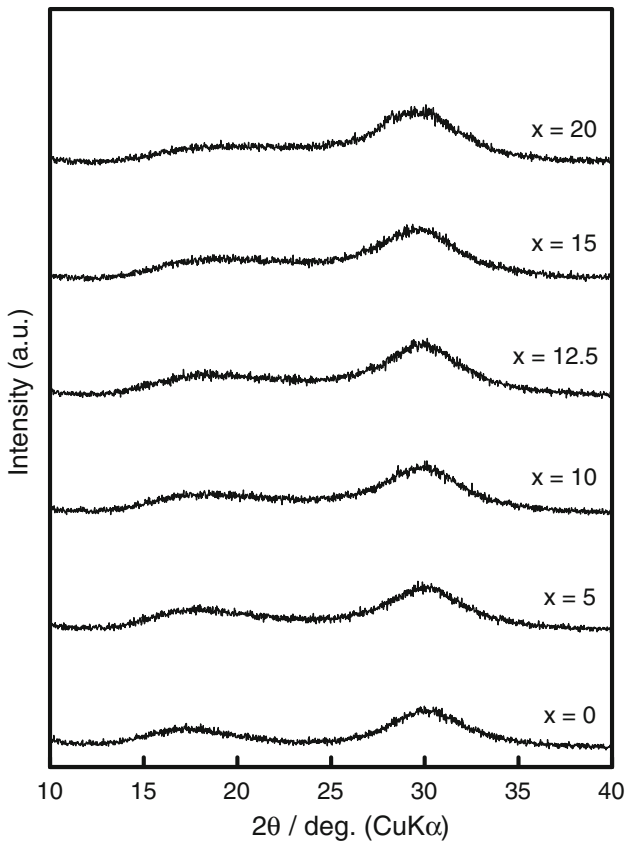

Fig. 1 XRD patterns of the $(100 - x)(0.7Li_2S{\cdot}0.3P_2S_5){\cdot}x$LiBr samples prepared by milling for 10 h

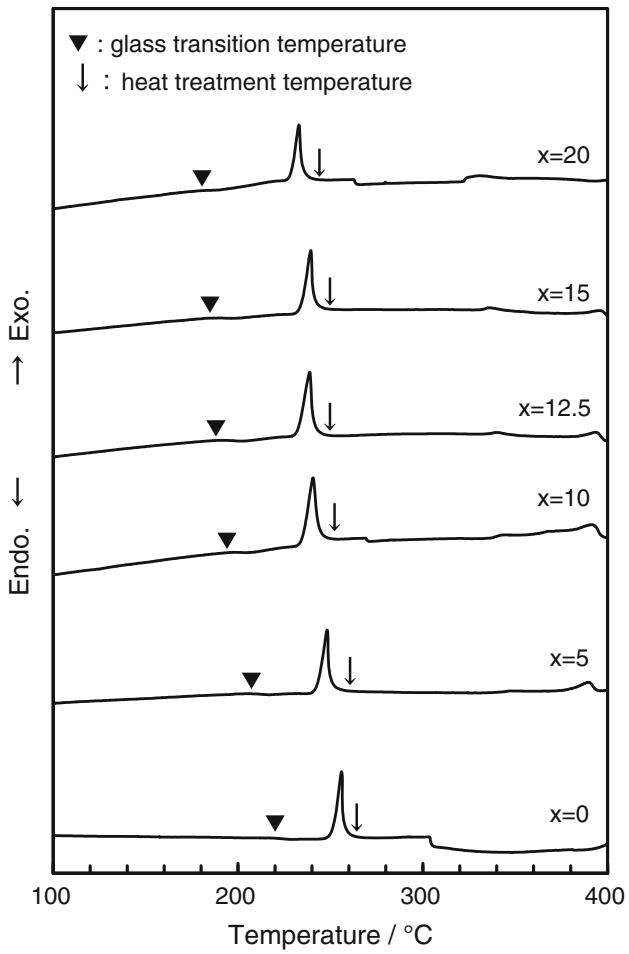

Fig. 2 DTA curves of the $(100 - x)(0.7Li_2S{\cdot}0.3P_2S_5){\cdot}x$LiBr samples prepared by milling for 10 h

glass composition and the glass structure. Results suggest that the milled LiBr was not simply amorphous, but mainly entered into the binary Li_2S–P_2S_5 glass.

The XRD patterns of the $(100 - x)(0.7Li_2S{\cdot}0.3P_2S_5){\cdot}x$LiBr samples prepared using heat treatment are depicted in Fig. 3. Several crystalline peaks were observed, indicating that glass–ceramics were obtained. The $Li_7P_3S_{11}$ crystals with high lithium ion conductivity were precipitated in all samples. The $Li_7P_3S_{11}$ crystal peaks maintained almost identical intensity in the composition range from $x = 0$ to 15. At $x = 20$, the intensity of the peaks of the $Li_7P_3S_{11}$ crystal was weakened slightly, suggesting that the $Li_7P_3S_{11}$ crystallinity was degraded. No marked shift of the peaks caused by the $Li_7P_3S_{11}$ crystal was observed. However, the formation of a solid solution of LiBr in the $Li_7P_3S_{11}$ crystal cannot be denied. Br^- ions would be partially substituted for S^{2-} ions to form a $Li_{7-x}P_3S_{11-x}Br_x$ crystal if LiBr is dissolved in the $Li_7P_3S_{11}$ crystal. The shift of the diffraction peaks caused by the solid solution must be slight because the ionic radii of Br^- and S^{2-} are close [15]. The little shift of the diffraction peaks would not be clearly observed using our laboratory XRD instruments. Further structural analyses are necessary to confirm the solid solution. The peaks attributable to LiBr crystal were also observed in samples containing LiBr as a starting material. The intensity of the peaks increased concomitantly with increasing LiBr content. The LiBr crystals in the glass–ceramics were not caused by starting crystals, but were precipitated from the glasses because the crystal phase of LiBr disappeared completely during mechanical milling, as shown in Fig. 1. The peaks at 26.5° were attributable to carbon paste (graphite) painted on the pellets to facilitate AC impedance measurements.

The composition dependence of electrical conductivities at 25 °C for the glasses and glass–ceramics are portrayed in Fig. 4. The glass conductivities increased concomitantly with increasing LiBr content. The conductivity at $x = 20$ was 3.1×10^{-4} S cm^{-1}. The increase of the conductivity is expected to result from the increased Li^+ ion content in the glasses. The glass–ceramic conductivities also increased concomitantly with increasing LiBr content between $x = 0$–10. The conductivity of the glass–ceramic at $x = 0$ was 3.9×10^{-3} S cm^{-1}. It increased to

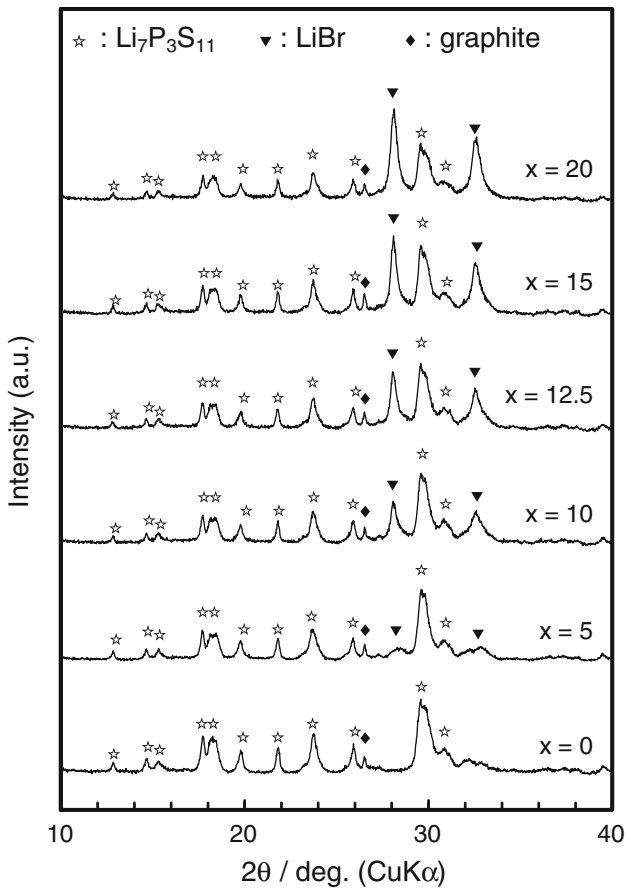

Fig. 3 XRD patterns of the $(100 - x)(0.7Li_2S{\cdot}0.3P_2S_5){\cdot}x$LiBr glass–ceramics prepared by milling for 10 h and subsequent heat treatment

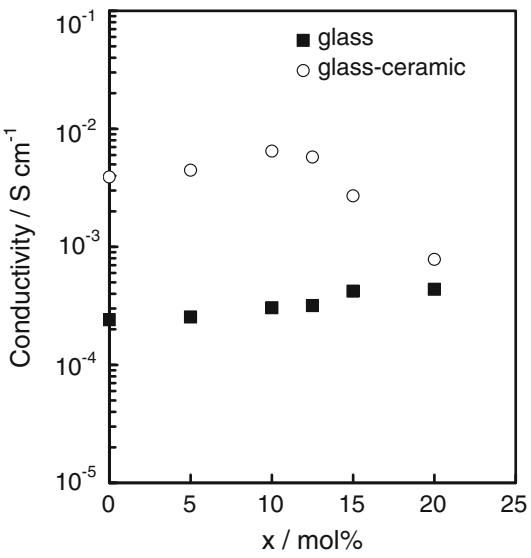

Fig. 4 Composition dependence of conductivities at 25 °C for the $(100 - x)(0.7Li_2S{\cdot}0.3P_2S_5){\cdot}x$LiBr glasses and glass–ceramics prepared by milling for 10 h and subsequent heat treatment

6.5×10^{-3} S cm^{-1} at $x = 10$. In the composition range of $x = 12.5$–20, the glass–ceramic conductivities were decreased concomitantly with increasing LiBr contents.

The change in the conductivity of glass–ceramic was inferred to result from the increased Li^+ ion content, the precipitation of the $Li_7P_3S_{11}$ crystal, and the precipitation of LiBr crystal. The increase in the Li^+ ion content would increase the conductivity of glass–ceramic because Li^+ ions are only charge carriers. The precipitation of $Li_7P_3S_{11}$ crystal provides high conductivity to glass–ceramic because the $Li_7P_3S_{11}$ crystal has extremely high conductivity [6]. The LiBr crystal precipitation would decrease the conductivity of glass–ceramic because of its low conductivity [17]. In the range of $x = 0$–10, the $Li_7P_3S_{11}$ crystal caused high conductivity of glass–ceramic. The Li^+ ions as charge carriers were increased by the non-crystallized LiBr component. Therefore, the conductivity of glass–ceramic was enhanced in spite of the precipitation of LiBr crystal. In addition, the possibility exists that a solid solution of LiBr in the $Li_7P_3S_{11}$ crystal improved the conductivity. In the range of $x = 12.5$–20, the $Li_7P_3S_{11}$ crystal provides high conductivity to glass–ceramic in the same manner between $x = 0$–10. However, the excessive increase in LiBr crystal decreased glass–ceramic conductivity despite the increase in the Li^+ ion content. In addition, at $x = 20$, the decrease in the conductivity was accelerated by the degradation of the $Li_7P_3S_{11}$ crystal crystallinity.

As portrayed in Fig. 4, the highest conductivity of 6.5×10^{-3} S cm^{-1} was obtained for the $90(0.7Li_2S{\cdot}0.3P_2S_5){\cdot}10$LiBr glass–ceramic. We sought to enhance the conductivity of the $90(0.7Li_2S{\cdot}0.3P_2S_5){\cdot}10$LiBr glass–ceramic by changing the milling process. Figure 5 shows the XRD patterns of the $90(0.7Li_2S{\cdot}0.3P_2S_5){\cdot}10$LiBr glasses prepared using various milling processes. The samples labeled as "10hMM", "20hMM", and "30hMM" were milled, respectively, for 10, 20, and 30 h. The samples labeled as "$(Li_2S + P_2S_5) + $LiBr", "$(LiBr + P_2S_5) + Li_2S$", and "$(Li_2S + $LiBr$) + P_2S_5$" were milled using two-step milling defined in "Experimental". Halo patterns were observed for all samples. Glasses were obtained despite the difference in milling processes. An unknown peak was observed for the $(Li_2S + $LiBr$) + P_2S_5$ sample, and also for the "$(Li_2S + $LiBr)" sample, suggesting that the peak resulted from a compound of Li_2S and LiBr. The peak assignment has not been clarified yet.

The DTA curves of the $90(0.7Li_2S{\cdot}0.3P_2S_5){\cdot}10$LiBr glasses prepared using various milling processes are depicted in Fig. 6. The exothermic peaks attributable to crystallization were observed between 220 and 230 °C. Glass transition phenomena were observed at about 195 °C in all samples. The glasses prepared by milling for over 20 h except for the $(Li_2S + $LiBr$) + P_2S_5$ glass showed a

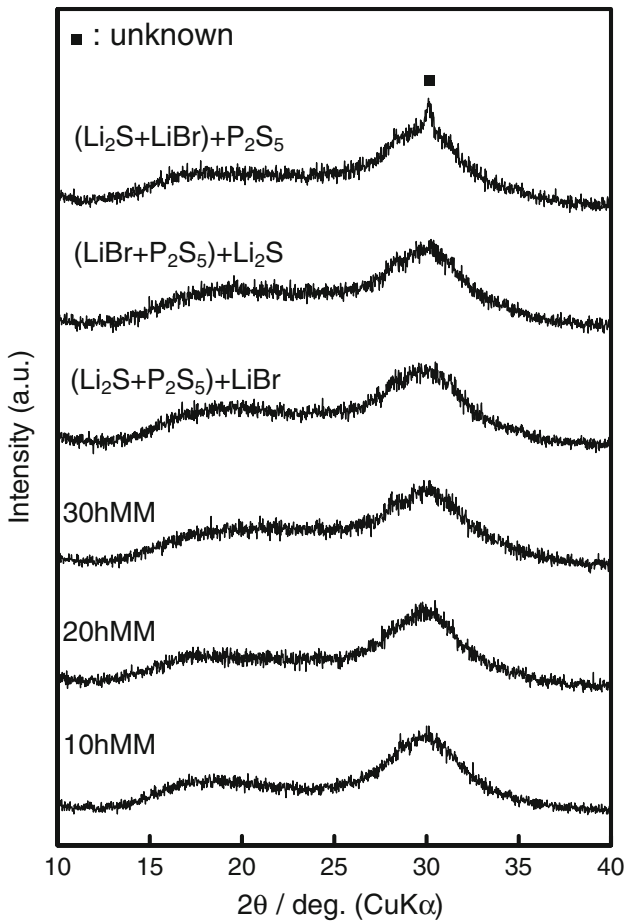

Fig. 5 XRD patterns of the $90(0.7Li_2S{\cdot}0.3P_2S_5){\cdot}10LiBr$ glasses prepared using various milling processes. The samples labeled as "10hMM", "20hMM" and "30hMM" were milled for, respectively, 10, 20 and 30 h. The samples labeled as "$(Li_2S + P_2S_5) + LiBr$", "$(LiBr + P_2S_5) + Li_2S$" and "$(Li_2S + LiBr) + P_2S_5$" were milled by the two-step milling

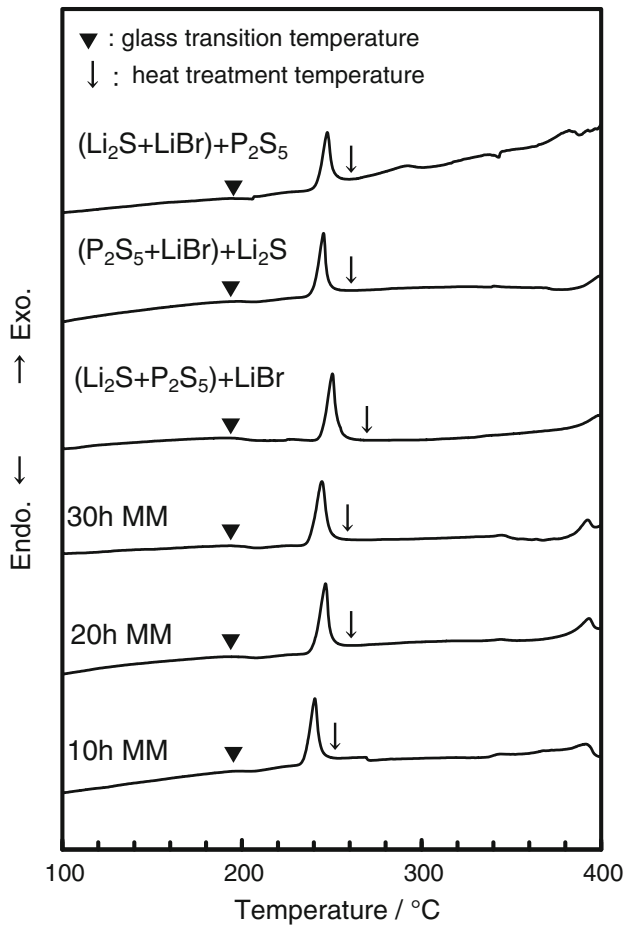

Fig. 6 DTA curves of the $90(0.7Li_2S{\cdot}0.3P_2S_5){\cdot}10LiBr$ glasses prepared using various milling processes

clearer glass transition than the 10hMM glass. Milling for 20 or 30 h was believed to be effective for obtaining homogeneous glasses [8].

Figure 7 shows XRD patterns of the $90(0.7Li_2S{\cdot}0.3P_2S_5){\cdot}10LiBr$ glass–ceramics prepared using various milling processes and subsequent heat treatment. Each sample was heated at a temperature between 250 and 270 °C. The peaks attributable to the $Li_7P_3S_{11}$ crystal and LiBr crystal were observed for all samples. The intensities of the peaks attributable to LiBr crystal in the 10hMM and $(Li_2S + P_2S_5) + LiBr$ samples were slightly larger than those in the other samples. Results suggest that the milling period for the compounds containing LiBr affected the LiBr crystal precipitation in the glass–ceramic. In the $(Li_2S + LiBr) + P_2S_5$ sample, the peak intensity in the $Li_7P_3S_{11}$ crystal was weakened. A peak attributable to Li_2S crystal was observed.

Table 1 shows the conductivities at 25 °C for the $90(0.7Li_2S{\cdot}0.3P_2S_5){\cdot}10LiBr$ glasses and glass–ceramics prepared using various milling processes and subsequent heat treatment. The $90(0.7Li_2S{\cdot}0.3P_2S_5){\cdot}10LiBr$ glass–ceramics milled for over 20 h showed extremely high conductivity of about 8×10^{-3} S cm^{-1}, except for the $(Li_2S + LiBr) + P_2S_5$ glass–ceramic. In the two-step milling samples, glass–ceramics with high conductivities tended to be obtained from glasses with high conductivities. The highest conductivity of 8.4×10^{-3} S cm^{-1} was obtained for the $(LiBr + P_2S_5) + Li_2S$ glass–ceramic. Results suggest that enhancement of the conductivity of the glass–ceramic resulted from improvement of the glass homogeneity. A highly homogeneous glass would decrease the precipitation of LiBr crystal with low conductivity. Low conductivity was obtained for the $(Li_2S + P_2S_5) + LiBr$ glass–ceramic. The $(Li_2S + P_2S_5) + LiBr$ glass–ceramic showed XRD peaks of LiBr crystal with a large intensity as portrayed in Fig. 7. Therefore, the growth of LiBr crystal would decrease the conductivity of the $(Li_2S + P_2S_5) + LiBr$ glass–ceramic. The lowest conductivity of the $(Li_2S + LiBr) + P_2S_5$ glass–ceramic would result from the degradation of the crystallinity of the

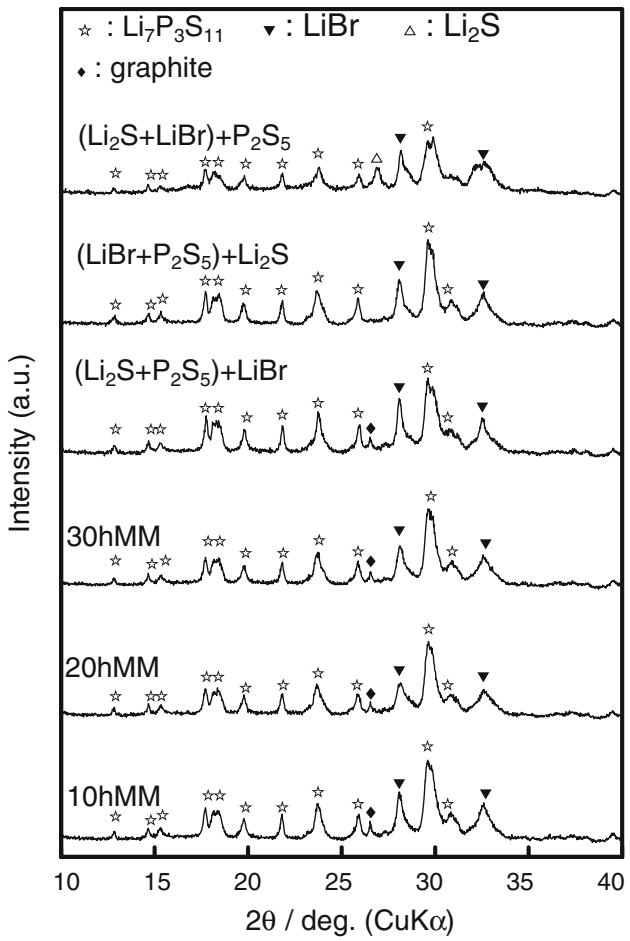

Fig. 7 XRD patterns of the $90(0.7Li_2S{\cdot}0.3P_2S_5){\cdot}10LiBr$ glass–ceramics prepared using various milling processes and subsequent heat treatment

Table 1 Conductivities at 25 °C for the $90(0.7Li_2S{\cdot}0.3P_2S_5){\cdot}10LiBr$ glasses and glass–ceramics prepared using various milling processes and subsequent heat treatment

Preparation conditions for $90(0.7Li_2S{\cdot}0.3P_2S_5){\cdot}10LiBr$ (mol %) samples		Conductivity (S cm^{-1})	
Sample	Milling time (h)	Glass	Glass–ceramic
$(Li_2S + LiBr) + P_2S_5$	20	2.4×10^{-4}	1.9×10^{-3}
$(LiBr + P_2S_5) + Li_2S$	20	3.4×10^{-4}	8.4×10^{-3}
$(Li_2S + P_2S_5) + LiBr$	20	2.9×10^{-4}	7.4×10^{-3}
30hMM	30	3.5×10^{-4}	7.7×10^{-3}
20hMM	20	3.4×10^{-4}	8.0×10^{-3}
10hMM	10	3.1×10^{-4}	6.5×10^{-3}

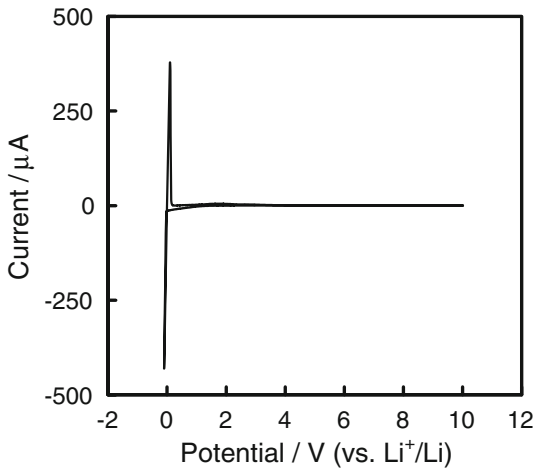

Fig. 8 Cyclic voltammogram of the $90(0.7Li_2S{\cdot}0.3P_2S_5){\cdot}10LiBr$ glass–ceramic electrolyte. The scan rate was 5 mV s^{-1}. The potential was swept between −0.1 and +10 V

$Li_7P_3S_{11}$ crystal and the precipitation of Li_2S crystal, as portrayed in Fig. 7. To obtain high conductivity for the $90(0.7Li_2S{\cdot}0.3P_2S_5){\cdot}10LiBr$ glass–ceramic, P_2S_5 as a network former of the glass should be mixed from the beginning of the vitrification process. The milling period of time for the vitrification should also be controlled to enhance the glass–ceramic conductivity, because the precipitation of LiBr crystal by heat treatment is affected by the milling period of time for the preparation of glasses.

The $90(0.7Li_2S{\cdot}0.3P_2S_5){\cdot}10LiBr$ glass–ceramic (20hMM) was used in the cells for cyclic voltammetry and charge–discharge measurement. Figure 8 shows the cyclic voltammogram of glass–ceramic. Large cathodic and anodic currents attributable to deposition and dissolution of lithium metal were observed in the potential range from −0.1 to +0.1 V vs. Li^+/Li. The glass–ceramic electrolyte exhibited a wide electrochemical window, because no obvious cathodic or anodic current was observed up to 10 V. Reportedly, the electrochemical stability range of $67Li_2S{\cdot}33P_2S_5$ glass added with LiI was about 2.9 V vs. Li^+/Li [18]. On the other hand, we reported a wide electrochemical window of $80(0.7Li_2S{\cdot}0.3P_2S_5){\cdot}20LiI$ glass up to 10 V vs. Li^+/Li [14]. The present study confirmed the high electrochemical stability of $90(0.7Li_2S{\cdot}0.3P_2S_5){\cdot}10LiBr$ glass–ceramic.

An all-solid-state cell using the $90(0.7Li_2S{\cdot}0.3P_2S_5){\cdot}10LiBr$ glass–ceramic electrolyte was fabricated. The charge–discharge curves of the all-solid-state cell are shown in Fig. 9. The cell was charged up to 3.6 V vs. Li–In and was discharged to 2.0 V vs. Li–In at the current density of 0.064 mA cm^{-2}. The cell showed an average voltage plateau at 3.3 V in both charge and discharge processes. The cell voltage of 3.3 V vs. Li–In corresponds to the potential of 3.9 V vs. Li^+/Li, which is the charge–discharge potential of $LiCoO_2$. The discharge capacity of 90 mAh g^{-1} was obtained at the first cycle. Coulombic efficiencies of greater than 95 % were obtained except for the first cycle, which indicated that the cell using the

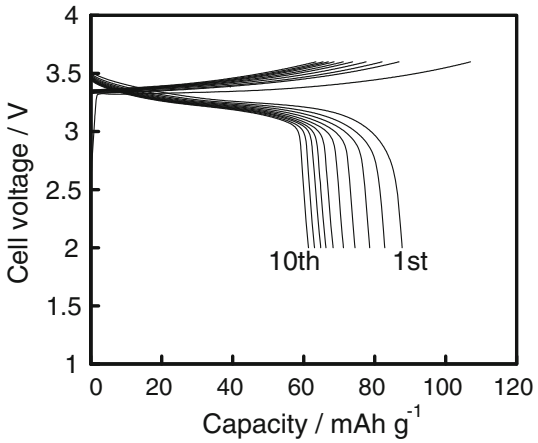

Fig. 9 Charge–discharge curves of the all-solid-state cell In/$90(0.7Li_2S{\cdot}0.3P_2S_5){\cdot}10LiBr$ glass–ceramic/$LiCoO_2$ at 25 °C. The cell was charged and discharged between 2.0 and 3.6 V at the current density of 0.064 mA cm^{-2}

$90(0.7Li_2S{\cdot}0.3P_2S_5){\cdot}10LiBr$ glass–ceramic electrolyte operated as a lithium secondary battery at room temperature. The capacity was decreased gradually with charge–discharge cycling. Decrease of the capacity with cycling was also observed for the cell using the $70Li_2S{\cdot}30P_2S_5$ glass–ceramic electrolyte without LiBr. Consequently, the added LiBr would not decrease the capacity. Results of TEM-EDX analysis indicated that sulfur and phosphorus in the electrolyte added to the composite electrode diffused to the $LiCoO_2$ active material [19]. The diffusion increased the interfacial resistances between the electrolyte and $LiCoO_2$ with cycling. The cycle performance of the cell would be improved using adequate active materials for the electrolyte [20]. The $90(0.7Li_2S{\cdot}0.3P_2S_5){\cdot}10LiBr$ glass–ceramic material with a high lithium ion conductivity is attractive as a solid electrolyte for a separator layer in all-solid-state batteries.

Conclusion

New electrolytes of $(100 - x)(0.7Li_2S{\cdot}0.3P_2S_5){\cdot}xLiBr$ ($x = 0$, 5, 10, 12.5, 15 and 20) were synthesized. Glass electrolytes were obtained by mechanical milling in the composition range of $x = 0$–20. The glass conductivity increased concomitantly with increasing LiBr content. The glass at $x = 20$ showed conductivity of 3.1×10^{-4} S cm^{-1}. Glass–ceramic electrolytes were prepared using heat treatment for the glasses. The $Li_7P_3S_{11}$ crystals with high lithium ion conductivity and LiBr crystals were precipitated in all glass–ceramic electrolytes with added LiBr. High conductivity of 6.4×10^{-3} S cm^{-1} was obtained at $x = 10$. Furthermore, the conductivity of the $90(0.7Li_2S{\cdot}0.3P_2S_5){\cdot}10LiBr$ glass–ceramic electrolyte was improved to 8.4×10^{-3} S cm^{-1} by controlling of the milling period used to prepare the precursor glass. The $90(0.7Li_2S{\cdot}0.3P_2S_5){\cdot}10LiBr$ glass–ceramic electrolyte showed a wide electrochemical window up to 10 V and functioned as an electrolyte for an all-solid-state lithium secondary battery.

References

1. Malugani, J.P., Robert, G.: Preparation and electrical properties of the 0,37 Li_2S-0,18P_2S_5-0,45LiI glass. Solid State Ion. **1**, 519–523 (1980)
2. Paradel, A., Ribes, M.: Electrical properties of lithium conductive silicon sulfide glasses prepared by twin roller quenching. Solid State Ion. **18–19**, 351–355 (1986)
3. Kennedy, J.H., Sahami, S., Shea, S.W., Zhang, Z.: Preparation and conductivity measurement of SiS_2-Li_2S glasses doped with LiBr and LiCl. Solid State Ion. **18–19**, 368–371(1986)
4. Zhang, Z., Kennedy, J.H.: Synthesis and characterization of the B_2S_3–Li_2S, the P_2S_5–Li_2S and the B_2S_3–P_2S_5–Li2S glass systems. Solid State Ion. **38**, 217–224 (1990)
5. Kanno, R., Murayama, M.: Lithium ionic conductor thio-LISICON. J. Electrochem. Soc. **148**, A742–A746 (2001)
6. Mizuno, F., Hayashi, A., Tadanaga, K., Tatsumisago, M.: High lithium ion conducting glass–ceramics in the system Li_2S–P_2S_5. Solid State Ion. **177**, 2721–2725 (2006)
7. Minami, K., Hayashi, A., Tatsumisago, M.: Electrical and electrochemical properties of the $70Li_2S{\cdot}(30–x)P_2S_5{\cdot}xP_2O_5$ glass–ceramic electrolytes. Solid State Ion. **179**, 1282–1285 (2008)
8. Hayashi, A., Minami, K., Ujiie, S., Tatsumisago, M.: Preparation and ionic conductivity of $Li_7P_3S_{11-z}$ glass–ceramic electrolytes. J. Non-Cryst. Solids. **356**, 2670–2673 (2010)
9. Minami, K., Hayashi, A., Tatsumisago, M.: Preparation and characterization of lithium ion conducting Li_2S–P_2S_5–GeS_2 glasses and glass–ceramics. J. Non-Cryst. Solids. **356**, 2666–2669 (2010)
10. Rao, R.P., Adams, S.: Studies of lithium argyrodite solid electrolytes for all-solid-state batteries. Phys. Status Solidi A. **208**, 1804–1807 (2011)
11. Homma, K., Yonemura, M., Kobayashi, T., Nagao, M., Hirayama, M., Kanno, R.: Crystal structure and phase transitions of the lithium ionic conductor Li_3PS_4. Solid State Ion. **182**, 53–58 (2011)
12. Boulineau, S., Courty, M., Tarascon, J.M., Viallet, V.: Mechanochemical synthesis of Li-argyrodite Li_6PS_5X (X = Cl, Br, I) as sulfur-based solid electrolytes for all solid state batteries application. Solid State Ion. **221**, 1–5 (2011)
13. Kamaya, N., Homma, K., Yamakawa, Y., Hirayama, M., Kanno, R., Yonemura, M., Kamiyama, T., Kato, Y., Hara, S., Kawamoto, K., Mitsui, A.: A lithium superionic conductor. Nat. Mater. **10**, 682–686 (2011)
14. Ujiie, S., Hayashi, A., Tatsumisago, M.: Structure, ionic conductivity and electrochemical stability of Li_2S–P_2S_5–LiI glass and glass–ceramic electrolytes. Solid State Ion. **211**, 42–45 (2012)
15. Shannon, R.D.: Revised effective ionic radii and systematic studies of interatomic distances in halides and chalcogenides. Acta. Cryst. **A32**, 751–767 (1976)
16. Ohta, N., Takada, K., Sakaguchi, I., Zhang, L., Ma, R., Fukuda, K., Osada, M., Sasaki, T.: $LiNbO_3$-coated $LiCoO_2$ as cathode material for all solid-state lithium secondary batteries. Electrochem. Commun. **9**, 1486–1490 (2007)

17. Mercier, R., Tachez, M., Malugani, J.P., Robert, G.: Effect of homovalent(I^-–Br^-)ion substitution on the ionic conductivity of $LiI_{1-x}Br_x$ system. Solid State Ion. **15**, 109–112 (1985)
18. Mercier, R., Malugani, J.P., Fahys, B., Robert, G.: Superionic conduction in Li_2S–P_2S_5–LiI–glass. Solid State Ion. **5**, 663–666 (1981)
19. Ohtomo, T., Hayashi, A., Tatsumisago, M., Tsuchida, Y., Hama, S., Kawamoto, K.: All-solid-state lithium secondary batteries using the $75Li_2S{\cdot}25P_2S_5$ glass and the $70Li_2S{\cdot}30P_2S_5$ glass–ceramic as solid electrolytes. J. Power Sour. **233**, 231–235 (2013)
20. Minami, K., Hayashi, A., Ujiie, S., Tatsumisago, M.: Electrical and electrochemical properties of glass-ceramic electrolytes in the systems Li_2S–P_2S_5–P_2S_3 and Li_2S–P_2S_5–P_2O_5. Solid State Ion. **192**, 122–125 (2011)